High-Directivity MEMS-Tunable Directional Couplers for 10-18 GHz Broadband Applications

Umer Shah, *Student Member, IEEE,* Mikael Sterner, and Joachim Oberhammer, *Senior Member, IEEE*

***Abstract*—This paper reports on two novel concepts of area-efficient, ultra-wideband, MEMS-reconfigurable coupled line directional couplers, whose coupling is tuned by mechanically changing the geometry of 3-D micromachined coupled transmission lines, utilizing integrated MEMS electrostatic actuators. Concept 1 is based on symmetrically changing the geometry of the ground coupling of each signal line, while Concept 2 is simultaneously varying both the ground coupling and the coupling between the two signal lines. This enables uniform and well predictable performance over a very large frequency range, in particular a constant coupling ratio while maintaining an excellent impedance match, along with high isolation and a very high directivity. For an implemented micromachined prototype 3-to-6 dB coupler based on Concept 1, the measured isolation is better than 16 dB, and the return loss and directivity are better than 10 dB over the entire bandwidth from 10 to 18 GHz. Concept 2 presents an even more significant improvement. For an implemented 10-to-20 dB prototype based on Concept 2, the measured isolation is better than 40 dB and the return loss is better than 15 dB over the entire bandwidth from 10 to 18 GHz for both states. The directivities for both states are better than 22 dB and 40 dB, respectively, over the whole frequency range. The measured data fits the simulation very well, except for higher through-port losses of the prototype devices. All devices have been implemented in an SOI RF MEMS fabrication process. Measured actuation voltages of the different actuators are lower than 35 V. Reliability tests were conducted up to 500 million cycles without device degradation.**

***Index Terms*—Tunable directional coupler, coupled-line coupler, RF MEMS, micromachined transmission line, micromachining.**

I. Introduction

RF power dividers/combiners and directional couplers are key elements in modern communication systems, including beam forming networks [1], power control amplifiers [2], MIMO systems, and adaptive antenna feedback mechanisms, which are getting more and more common to achieve high data throughput at limited power [3]. A directional coupler is a multi-purpose passive device used for sampling, splitting, combining or isolating signals. Directional couplers are one of the most often used components in microwave circuits [4]. The directivity of a directional coupler, the ratio between the output power on the coupled and the isolated port, is a particularly important measure of its quality [4], besides its insertion loss. However, it is difficult to realize integrated directional couplers with high directivities [4] and typically directivities between 15 dB and 20 dB are obtained for tunable couplers operating between 1-10 GHz frequency [2], [5]. Directional couplers that are designed for high directivity unfortunately exhibit poor bandwidth characteristics [6]. With the recent advent of multi-standard frontends in modern telecommunication systems [7], directional couplers capable of operating with different frequency bands [6], [8] and with tunable coupling ratio [9], [10] are of particular interest for future reconfigurable architectures. The tuning range of the coupling ratio is usually limited to only a few decibels [11]. When tuned beyond this coupling ratio range, the input matching and directivity degrade drastically. The directional coupler in [12] tries to overcome these problems but falls short in terms of bandwidth. Thus, novel concepts are required where the input matching and directivity is maintained while the coupling ratio is tuned over a large, for instance 10 dB, range.

Previous attempts of tunable couplers consist of MMIC based active couplers [5], [13], [14] and varactor diode based passive couplers [10]–[12], [15], [16], and are predominantly designed for operating below 8 GHz.

RF MEMS components are especially of interest for reconfigurable/tunable circuits for frequency agile front end applications, due to their near-ideal signal handling behavior, ultra-low power consumption, low loss, large bandwidth and the potential of low-cost production and easiness of integration, since fabrication is compatible to integrated circuits. Micromechanically tunable parallel-plate capacitor with electrostatic actuation designs are easily implemented with standard surface micromachining thin-film technology [17]. MEMS fabrication technology has also proven to be very suitable for creating on-wafer three-dimensionally (3-D) micromachined transmission lines which offer reduced substrate and radiation losses as compared to conventional coplanar or microstrip lines [18], [19].

Despite MEMS being known for creating very low-loss tuning mechanisms, there have been very few attempts of implementing MEMS-based tunable couplers. A MEMS power divider concept based on two cascaded hybrid couplers was presented in [20]. This concept occupies a very large area. Coupled line directional couplers on the other hand can be designed much more space-efficient, and to our knowledge, so far only one research paper has reported on a MEMS-switched coupled line directional coupler concept [21]. Unfortunately, the data reported was incomplete (through-port data was not provided) for judging the overall performance of this MEMS-switched directional coupler.

The authors have previously shown the integration of tunable capacitors [22] and switches [23] based on an electrostatic actuation mechanism embedded inside the ground layer of a 3-D micromachined coplanar transmission line. This results in a minimized line discontinuity and fabrication is done by

The authors are with the Micro and Nanosystems, School of Electrical Engineering, KTH Royal Institute of Technology, Stockholm SE-100 44, Sweden (e-mail: umers@kth.se; msterner@kth.se; joachim.oberhammer@ee.kth.se).

Manuscript received XXXXX; revised XXXXX

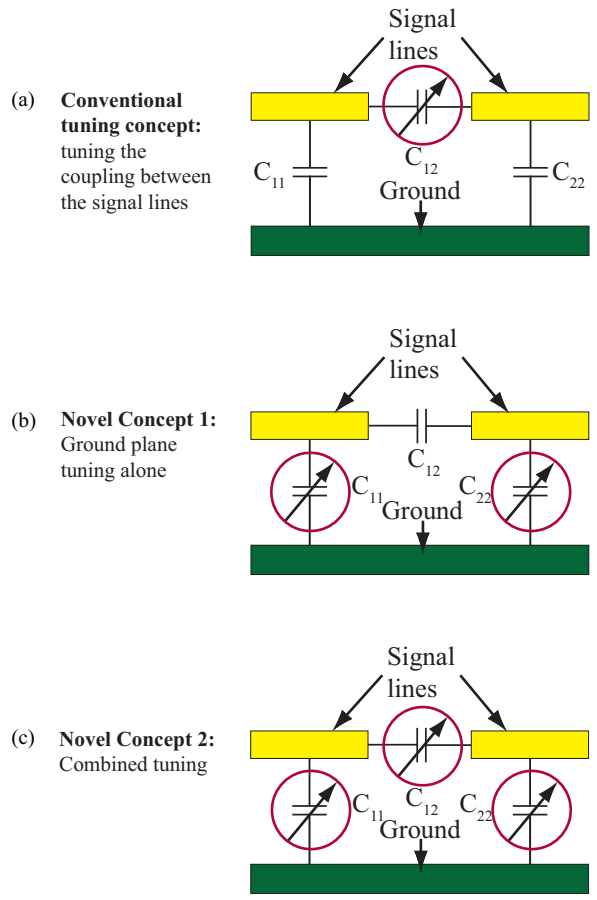

Fig. 1. Basic working principle of: (a) conventional tunable coupled line directional couplers; (b) novel Concept 1; and (c) novel Concept 2 of the MEMS tunable coupled line directional couplers presented in this paper.

a single-mask silicon on insulator (SOI) RF MEMS process developed by the authors. The present paper reports on two novel concepts of coupled line directional couplers whose coupling is tuned by mechanically changing the geometry of 3-D micromachined coupled transmission lines. In contrast to conventional designs, the coupling is achieved by tuning both the ground and the signal line coupling, obtaining a large tunable-coupling ratio while maintaining an excellent impedance match and directivity over a so far unreported wide bandwidth, and thus overcoming the afore mentioned problems of conventional approaches. The authors have presented these concepts for the first time at a conference [24]. The present paper discusses the novel concepts in detail and presents new characterization and simulation data.

II. Concept and Design

A. Basic design of tunable coupled line directional couplers

The basic principle of a coupled line directional coupler is shown in Fig. 1. RF power is coupled between two unshielded transmission lines due to the interaction of the electromagnetic field when the lines are in close proximity [25]. Typically, a substantial part of the coupling happens via a third conductor, i.e. a common ground layer. These lines are assumed to operate in TEM mode and their electrical coupling characteristics can be completely determined by the effective capacitances between the three conductors, as shown in Fig. 1. C_{11} is the capacitance of line 1 to the ground, C_{22} is the capacitance of line 2 to the ground, and C_{12} is the capacitance between the two lines. If the geometry is symmetrical, i.e. the two signal lines have the same size and location relative to the ground layer, then $C_{11} = C_{22}$. Even and odd mode excitation of the coupled lines reveal that both the even and odd mode capacitances are strongly influenced by the capacitance to ground of each signal line. The even and odd mode capacitances can be written as [25]

$$C_{\text{even}} = C_{11} = C_{22} \tag{1}$$

$$C_{\text{odd}} = C_{11} + 2C_{12} = C_{22} + 2C_{12} \tag{2}$$

This results in a strong dependence of the characteristic impedances of the even and odd modes on capacitance of each line to ground [25].

$$Z_{0,\text{even}} = \sqrt{\frac{L}{C_{\text{even}}}} = \frac{1}{v_p C_{\text{even}}} \tag{3}$$

$$Z_{0,\text{odd}} = \sqrt{\frac{L}{C_{\text{odd}}}} = \frac{1}{v_p C_{\text{odd}}} \tag{4}$$

where v_p is the phase velocity of propagation on the line. This analysis assumes that the lines are symmetric and that fringing capacitances are identical for even and odd modes. Since the overall coupling can be represented in terms of even and odd mode impedance [25], the total coupling between the lines can be changed by either changing the coupling between the signal lines or the coupling of each signal line to the ground or both:

$$C = \frac{Z_{0,\text{even}} - Z_{0,\text{odd}}}{Z_{0,\text{even}} + Z_{0,\text{odd}}} \tag{5}$$

In the above analysis, it was assumed that the even and odd modes have the same propagation velocities so that the line has the same electrical length for both modes. For a non-TEM line, for instance a quasi-TEM coplanar waveguide transmission line, this condition will generally not be satisfied, which leads to a coupler design with poor directivity [25]. The characteristic impedance of the line is $Z_0 = \sqrt{Z_{0,\text{even}} Z_{0,\text{odd}}}$. Thus for controlling the coupling and the line matching independently, $Z_{0,\text{even}}$ and $Z_{0,\text{odd}}$ and thus C_{even} and C_{odd} should ideally be controlled independently.

B. Conventional and novel concepts of coupled line tunable directional couplers

Fig. 1(a) shows the principle of the conventional concept of changing the coupling between two coupled lines in a directional coupler by varying the capacitance C_{12} between the two signal lines without changing the ground capacitances C_{11} and C_{22}. Fig. 1(b) and Fig. 1(c) illustrate the two novel tuning concepts of coupled line directional couplers presented in this paper:

1) Concept 1: In the equivalent capacitance model, the coupling is varied by changing the capacitances C_{11} and C_{22} of the signal lines to the ground and the capacitance C_{12} between the signal lines is not changed. In contrast to the

conventional tuning concept, where only the odd-mode capacitance is changed but the even-mode capacitance is kept constant, for Concept 1 both the even and the odd-mode capacitances are changed when varying the ground capacitances. A 3-D illustration of Concept 1 (Fig. 1(b)) is shown in Fig. 2. Here, the ground-coupling of the signal lines is varied by laterally moving the ground sidewalls of the coupled coplanar waveguides using integrated MEMS electrostatic actuators, as shown in Fig. 3. For the prototypes implemented in this paper, the switching between the two states of the tunable couplers is achieved by moving floating ground conductors and connecting them to the RF ground in their end position. Thus, the nominal coupling is changed from 3 dB in State 1 to 6 dB in State 2. Actuation voltage only needs to be applied for one of the two states (active pull-in, passive release). This concept, similar to the conventional tuning concept, does not maintain the input match and directivity over a large bandwidth and for large tunable coupling ratios.

2) Concept 2: In the equivalent capacitance model, the coupling is varied by changing the capacitances C_{11} and C_{22} of the signal lines to the ground and simultaneously varying the capacitance C_{12} between the signal lines. This allows for controlling the even and the odd-mode capacitances independently and thus ideally allows to eliminate any impedance mismatch which cannot be achieved neither with the conventional concept nor with Concept 1. The coupling is varied by changing the capacitances C_{11} and C_{22} of the signal lines to the ground and simultaneously varying the capacitance C_{12} between the signal lines. As illustrated in Fig. 4, two narrow intermediate floating lines are switched to the signal lines of the two coupled lines, and simultaneously the ground sidewalls are moved apart for compensating the ground coupling, as shown in Fig. 5. This allows to design for a much larger coupling ratio variation by maintaining uniform performance over a large bandwidth. The prototype devices designed following Concept 2 demonstrate the large range of the tunable coupling ratio, and is implemented for varying the nominal coupling from 20 dB in State 1 to 10 dB in State 2. Concept 2 needs actuation voltages to be applied for both states, as the two independent actuators are operated alternatively for maintaining the two states. The novel Concept 2 maintains the input match and directivity of the coupler over a wide bandwidth, and simultaneously achieves a large tuning ratio. Concept 2 can achieve tight coupling (3 or 6 dB) which requires the coupled transmission lines to be close together. As long as the combination of even and odd mode characteristic impedances are physically realizable and it is possible to fit all the actuators and electrodes in the space between the two transmission lines, tight coupling could also easily be achieved with this concept.

The prototype implementations in this paper are designed as switched couplers, i.e. as two-state and not analog-tunable devices.

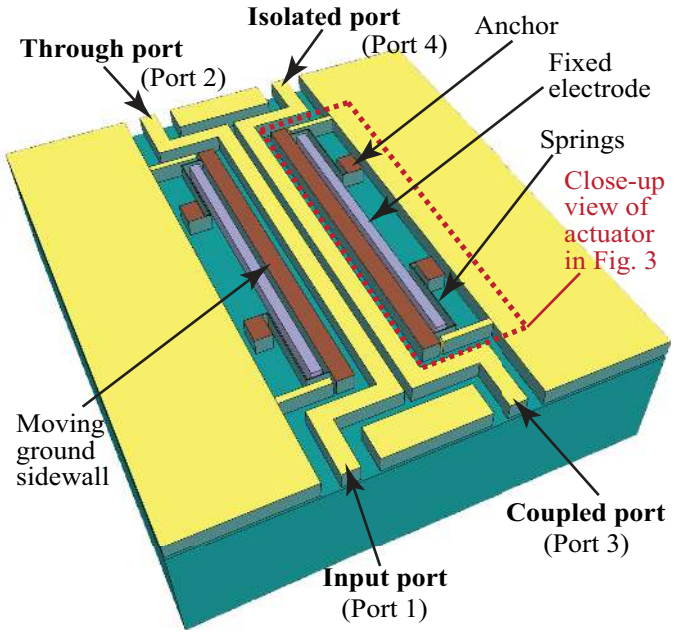

Fig. 2. Illustration of Concept 1, an ultra-wideband coupled line directional coupler based on geometrically tuning of the signal-to-ground coupling of the coupled lines.

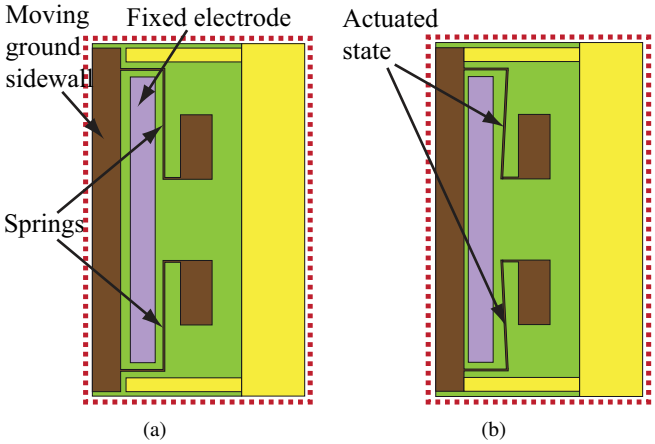

Fig. 3. Actuation states of Concept 1 (only one side of the coupled signal line illustrated): (a) State 1 (3 dB coupling); and (b) State 2 (6 dB coupling).

III. 3-D Transmission Line Metallization Schemes

The concept of the 3-D micromachined transmission lines implemented in this paper is shown in Fig. 6. Fig. 6(a) shows a conventional 2-D coplanar waveguide [26]. In contrast to that, for the 3-D micromachined coplanar waveguide of Type A, as shown in Fig. 6(b), the major part of the electric field lines is above the substrate which decreases dielectric losses and radiation losses into the substrate, and also the metallic losses are decreased since the currents, confined by the skin-depth to just the edges of the conductors, have a much larger volume available due to the extension in the vertical direction. A further variant is the 3-D micromachined coplanar waveguide Type B, shown in Fig. 6(c), which has metallization only on top of the 3-D topography. Both types

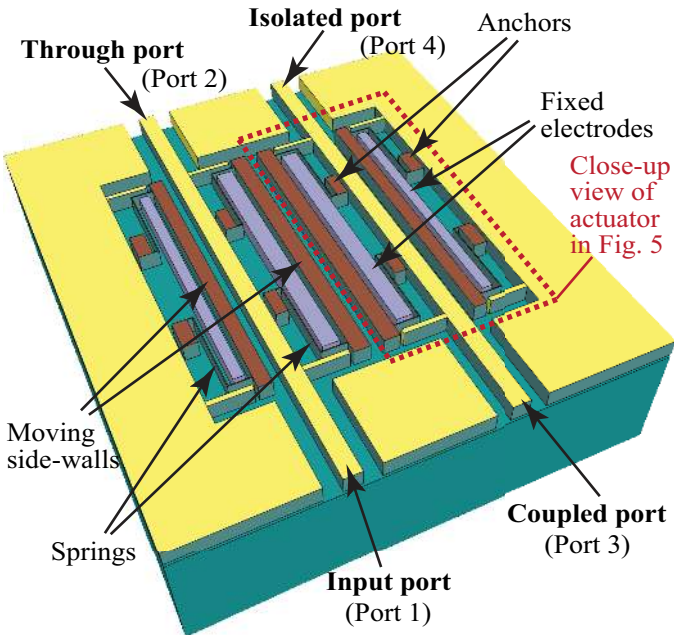

Fig. 4. Illustration of Concept 2, an ultra-wideband coupled line directional coupler based on geometrically tuning of the signal-to-ground coupling simultaneously with the signal-to-signal line coupling.

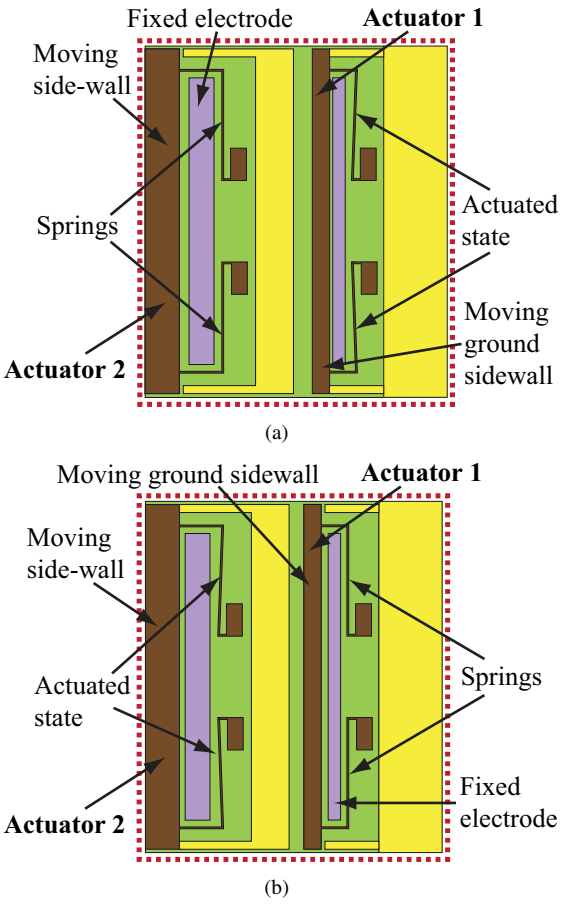

Fig. 5. Actuation states of Concept 2 (only one side of the coupled signal line illustrated): (a) State 1 (20 dB coupling); and (b) State 2 (10 dB coupling).

are investigated in this paper. Note that the geometry of the

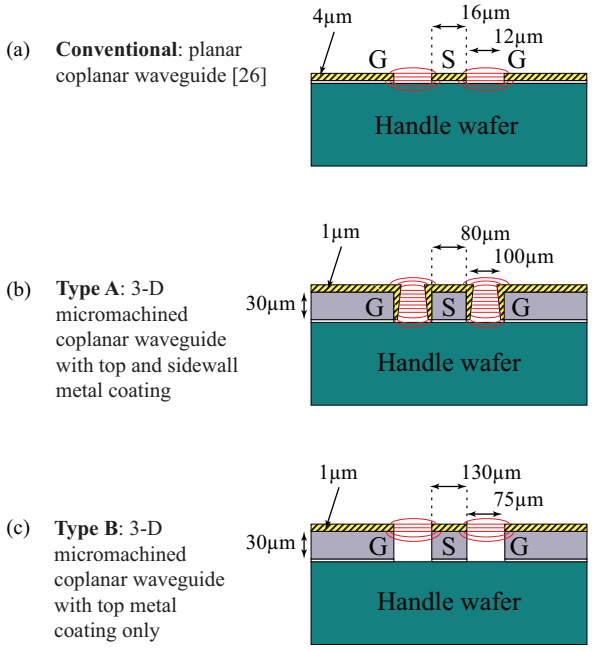

Fig. 6. Comparison of: (a) conventional 2-D coplanar waveguide; (b) 3-D micromachined coplanar waveguide of Type A with metallization layer on the sidewalls; and (c) 3-D micromachined coplanar waveguide of Type B with metallization only on the top layer.

slot widths of the two types is different for achieving the same characteristic impedance, as the geometry of Type A results in higher capacitance.

Fig. 7 compares the measurement results from 3-D micromachined coplanar waveguide of Type A and Type B. The fabricated overall transmission line length was 1 mm including the probe pads. The dimensions for the transmission lines are shown in Fig. 6. At 10 GHz, the insertion loss of the 3-D micromachined transmission line of Type B is 0.2 dB/mm while that of a conventional coplanar waveguide is 0.25 dB/mm [26]. Fig. 7 also shows that the 3-D micromachined transmission line of Type A is clearly more lossy than the 3-D micromachined transmission line of Type B. At 20 GHz, for instance, the insertion loss of transmission line of Type A is 1.17 dB/mm while that of Type B is 0.38 dB/mm despite better impedance match of the transmission line of Type A (lower S_{11}). The reason was that the sidewall metallization on transmission line of Type A was found to be very thin, as a sputtering metallization of 1 μm only resulted in a sidewall thickness of approximately 100 nm, which drastically increases the losses, as this thickness is by far below the skin depth. These higher losses can be attributed to conductor losses, as the RF reflections are insignificant. Due to the low loss characteristic, the 3-D micromachined transmission line of Type B is chosen to fabricate all directional coupler prototypes in this paper i.e. the metallization is only applied on top of the 3-D topography. The measured characteristic impedance for the transmission line of Type B (Fig. 6(c)) is 59 Ω and the effective dielectric constant derived from the measurements is 4.4.

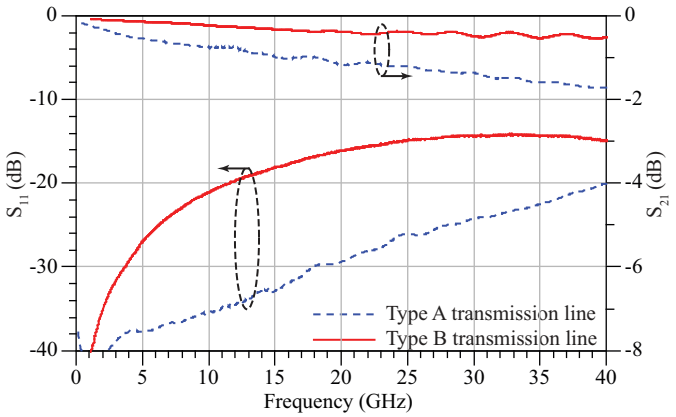

Fig. 7. Comparison of RF characterization of 3-D micromachined coplanar waveguides of Type A (with metallization layer on the top and on the sidewalls) and Type B (with metallization only on the top).

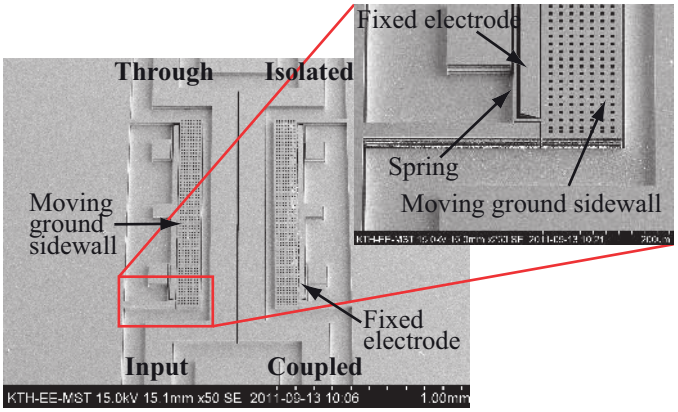

Fig. 8. SEM pictures of fabricated MEMS-tunable coupled line directional coupler of Concept 1, in 3-to-6 dB implementation, including a close-up view of the actuator.

IV. Fabrication

All structures are fabricated in a single-mask SOI RF MEMS process developed by the authors [23]. A high resistivity $> 3000\ \Omega$-cm SOI wafer is used with a device layer thickness of $30\,\mu$m, a buried oxide layer of $3\,\mu$m and a handle wafer thickness of $500\,\mu$m. The SOI device layer is structured by deep reactive ion etching (DRIE) followed by free etching the moving structures by wet etching the buried oxide layer using hydrofluoric acid. The top metallization is achieved by highly directional e-beam evaporation of a $1\,\mu$m thick gold layer using 50 nm of titanium as adhesion layer, followed by a short wet etch-back in order to remove potential deposition traces on the sidewalls. Finally, the metal coating on the substrate and in the unwanted areas is removed by electrochemically assisted selective etching of gold in an electrically biased potassium iodide and sodium sulfite solution [27]. All the wet steps are followed by critical point drying step. Fig. 8 shows a SEM picture of the fabricated prototype device based on Concept 1. The figure shows the complete device including input, through, coupled and isolated ports along with the fixed electrode and the moving ground sidewalls. It also shows the close up of the actuator design with the restoring springs, fixed electrode and the moving ground sidewall which can be switched for the desired coupler configuration. Similarly the SEM picture of fabricated prototype device based on Concept 2 is shown in Fig. 9.

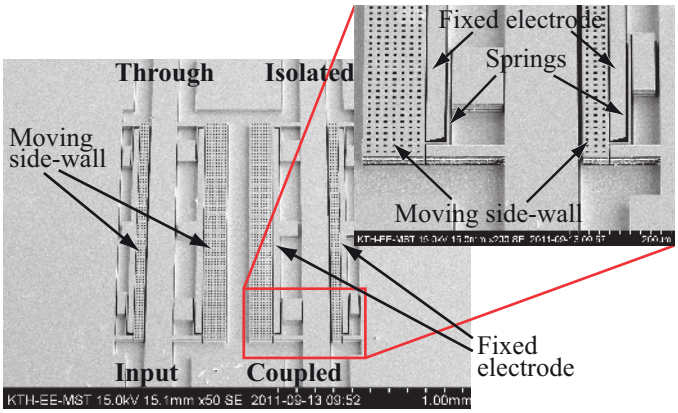

Fig. 9. SEM pictures of fabricated MEMS-tunable coupled line directional coupler of Concept 2, in 10-to-20 dB implementation, including a close-up view of the actuator.

V. Simulation and Characterization Results

All simulations were performed with Ansys HFSS, taking into account the dielectric losses in silicon ($> 3000\ \Omega$-cm) and the metallic losses in the gold films. Multi-mode simulation was carried in order to investigate the effect of mode conversion and associated losses. The couplers are designed for 10 to 18 GHz bandwidth imposing the maximally flat condition exhibiting a flat frequency response without resonances over their frequency range with the coupling flatness of ± 1.25 dB.

Since the RF measurements of the fabricated four-port directional couplers were performed on a two-port Agilent E8361A PNA network analyzer, three devices were fabricated of each type, where two ports out of the isolated, coupled, and through port were terminated on-chip with $50\ \Omega$ microwave thin film resistors in different combinations. Fig. 10 shows one of the three combinations, here for measuring the through port, i.e. with the isolated and the coupled ports terminated. Similarly, to measure the coupled port, the through and the isolated ports are terminated on a second device, and to measure the isolated port, the through and the coupled ports are terminated. The termination resistors used are commercially available 0201 SMD resistors (Vishay CH02016), with a size of $0.48 \times 0.39 \times 0.42$ mm^3, tolerance of 2%, maximum power of 30 mW, and an absolute impedance variation, taking into account the parasitics, of maximum 3% from $50\ \Omega$ over the whole frequency spectrum of DC to 50 GHz, and of better than 1% up to 20 GHz, according to the data sheet [28]. The resistors were mounted on the 3-D-micromachined transmission lines by using conductive silver-paste epoxy. Such kind of commercially available 0201 SMD resistors have been successfully used as termination resistors for millimeter wave application without any degradation in the RF performance with the resistors being mounted using conductive epoxy [29].

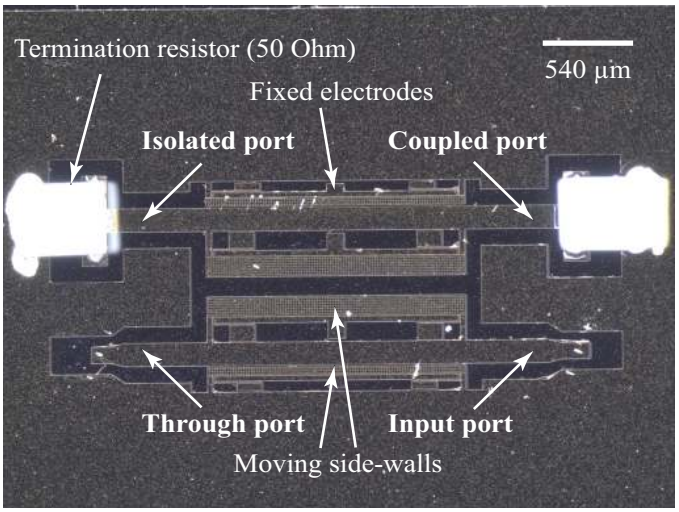

Fig. 10. Microscope photograph of a prototype device of Concept 2 in through-port measurement configuration, i.e. with the isolated and coupled port terminated by 50Ω microwave-grade SMD resistors.

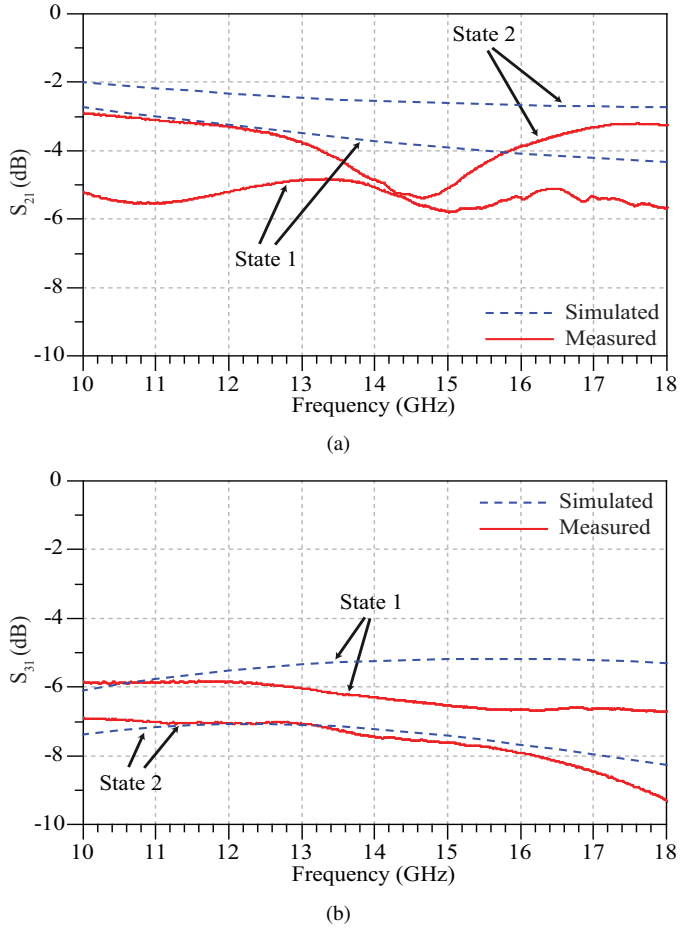

Fig. 11. Measured and simulated S-parameters in the two coupling states of 3-to-6 dB directional coupler (Concept 1): (a) through (S_{21}) port; and (b) coupled (S_{31}) port.

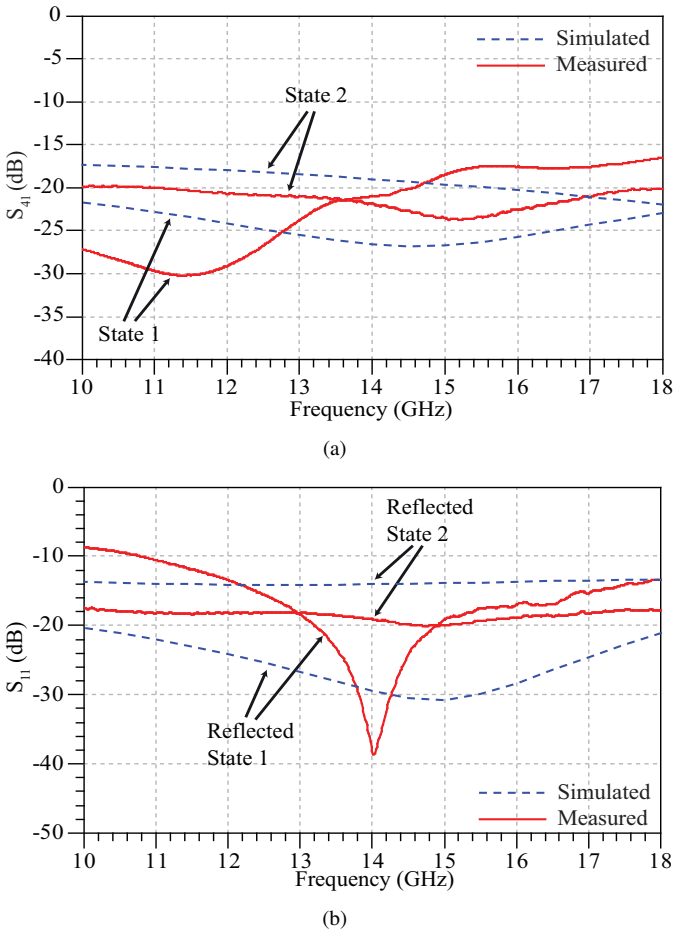

Fig. 12. Measured and simulated S-parameters in the two coupling states of 3-to-6 dB directional coupler (Concept 1): (a) isolated (S_{41}) port; and (b) return loss (S_{11}).

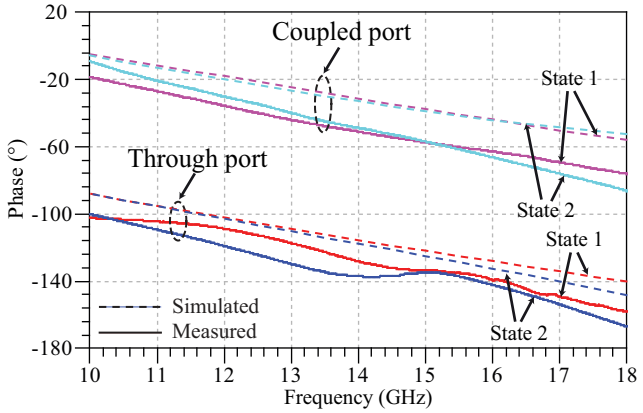

Fig. 13. Measured and simulated phase plots of coupled (S_{31}) and through (S_{21}) ports in the two coupling states of 3-to-6 dB directional coupler (Concept 1).

A. Results of Concept 1: tuning of signal-to-ground coupling

Measurement and simulation results of the through and coupled ports for the prototype of Concept 1 are shown in Fig. 11. The tunable coupled line directional coupler prototype, utilizing reconfigurable signal-to-ground-plane coupling only, is designed as a two-state 3-to-6 dB reconfigurable directional coupler. The simulation results show good wideband performance with the isolation being better than 17 dB in State 2 and better than 21 dB in State 1, for a very large bandwidth from 10 to 18 GHz. The device works as intended, but the measured through and coupled power levels fall short

by $1-2$ dB from the simulated values. For these types of circuits, the right angle bends can lead to performance degradation due to slot-line mode excitation, which increases the radiation loss in the circuit. The reactance of the bend itself can increases radiation loss which can be compensated by using chamfered corners. Furthermore, any step change in the width of the signal lines and ground gap can perturb the normal coplanar waveguide electric and magnetic fields, resulting in radiation loss besides impedance mismatch [30]. However, losses through mode conversion and radiation should also be seen in the simulations, since a multi-mode analysis was carried out. Furthermore, it was found that air bridges placed near the coplanar waveguide bends to suppress the parasitic slot line mode do not significantly improve the loss performance. The difference between measured and simulated pure transmission lines does not amount to more than 0.12-0.14 dB additional losses (10-18 GHz) derived from reference line measurements. Current crowding around the etch holes (features not implemented in the simulation model) can also be ruled out as a source of the losses as the moving elements are almost current-free in some states. Therefore, it is assumed that the additional losses are mainly attributed to the mounting of the termination resistors, since the simulation model uses ideal port termination for all four ports. The measured isolation is better than 20 dB in State 2 compared to being better than 16.5 dB in State 1 shown in Fig. 12(a). Fig. 12(b) shows good agreement between simulated and measured return loss trends in particular for State 2 with a measured return loss of better than 17.5 dB. The measured return loss for State 1 is better than 15 dB in the frequency band of 12 to 17 GHz. It is clear from the simulation and measurement results that both the high isolation and impedance match cannot be maintained over the entire frequency band of 10 to 18 GHz, similar to conventional tunable directional couplers tuning the signal-to-signal line coupling. Fig. 13 illustrates the measured and simulated phase plots for the through and coupled ports. The measured curve follows the simulated trend very well, considering that the absolute phase value is of no relevance as it depends on the reference plane. The simulated phase plot shows 90° difference between the coupled and through port with the maximum phase deviation from the ideal response (90°) being 8° in either actuation state. The measured maximum deviation of the phase difference from the ideal response is 17° in either actuation state.

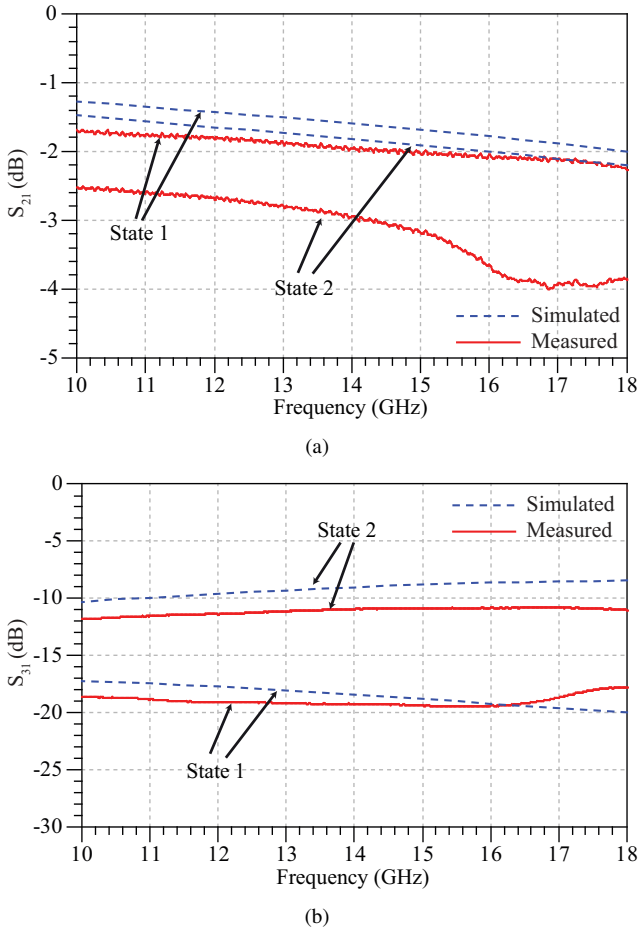

Fig. 14. Measured and simulated S-parameters in the two coupling states of 10-to-20 dB directional coupler (Concept 2): (a) through (S_{21}) port; and (b) coupled (S_{31}) port.

B. Results of Concept 2: simultaneous tuning of signal-to-ground and signal-to-signal coupling

As anticipated in the concept discussion, further tuning complexity has to be added to the coupled line directional coupler to maintain a good impedance match and high isolation over a wide bandwidth. This is implemented in Concept 2, whose prototype is designed as a two-state 10-to-20 dB reconfigurable coupler. The measurement and simulation results for the through and coupled ports are shown in Fig. 14. The measurement data of the through and coupled ports agree well with the design values. The overall excellent performance of the device is emphasized by the very uniform measurement characteristics over the whole 10 to 18 GHz spectrum for both states. The measured isolated port, shown in Fig. 15(a), is better than 40 dB for both states, and the measured return loss, shown in Fig. 15(b), is better than 15 dB through the entire frequency band of interest. The simulated and measured performance agree very well in all parameters, except that the measured device has higher losses, which is visible by the through-port power falling short by approximately 1-2 dB, for similar reasons as for Concept 1. Fig. 16 illustrates the measured and simulated phase plots for the through and coupled ports. The simulated phase plot shows the maximum phase deviation from the ideal response (90°) being 15° in State 2. In State 1, however, the measured phase response difference is not uniform over the whole band. The measured maximum deviation of the phase difference from the ideal response is 27° in State 2. In State 1 the measured phase response difference is not uniform over the whole band, in particular above 15 GHz. The overall excellent results of the Concept 2 prototype prove the performance benefit of the novel method of combined tuning of both the ground plane and signal-line coupling for achieving high performance and maintaining it over a large bandwidth.

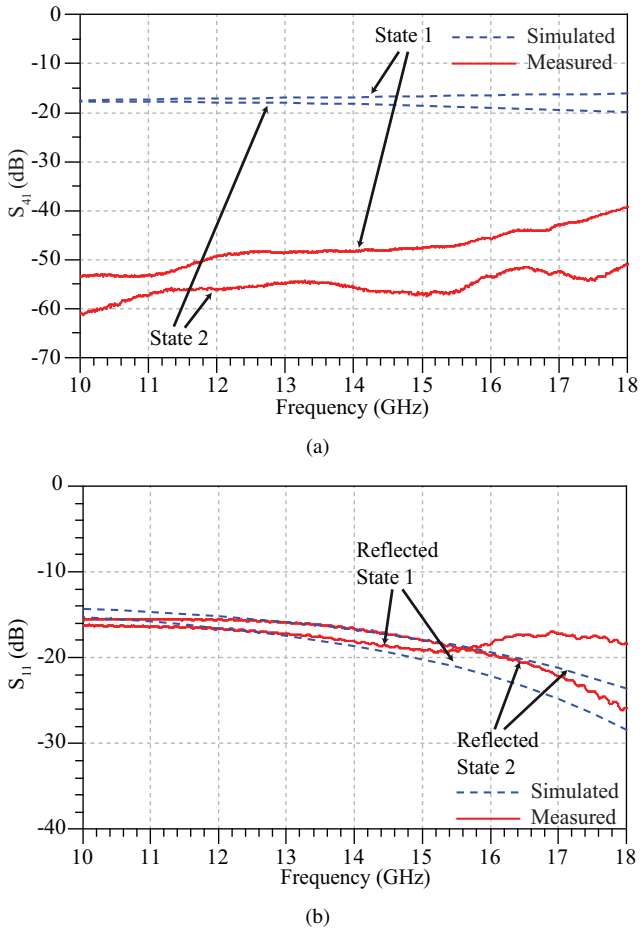

Fig. 15. Measured and simulated S-parameters in the two coupling states of 10-to-20 dB directional coupler (Concept 2): (a) isolated (S_{41}) port; and (b) return loss (S_{11}).

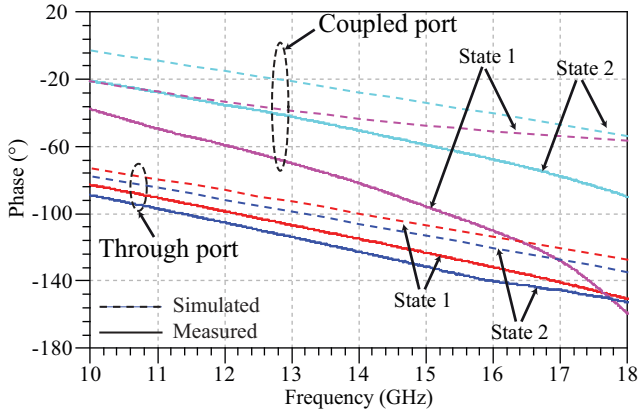

Fig. 16. Measured and simulated phase plots of coupled (S_{31}) and through (S_{21}) ports in the two coupling states of 10-to-20 dB directional coupler (Concept 2).

C. Directivity Analysis

The couplers are ultra-wide band, in contrast to all previously reported tunable couplers, with a 57% bandwidth from 10 to 18 GHz. Both novel concepts presented in this paper are very area-efficient with a size of $0.09\lambda \times 0.06\lambda$ at the center frequency in terms of free space wavelength area. This is comparable in size to the only previously published

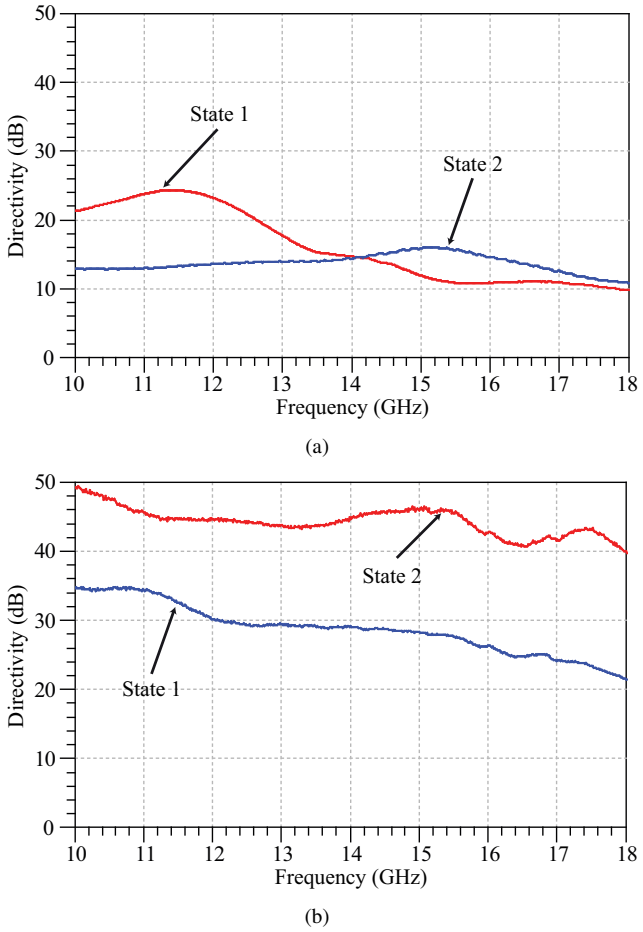

Fig. 17. Measured directivity for the fabricated directional couplers in the two coupling states: (a) 3-to-6 dB directional coupler (Concept 1); and (b) 10-to-20 dB directional coupler (Concept 2).

MEMS tunable coupled line directional coupler with a size of $0.08\lambda \times 0.07\lambda$ [21] at the center frequency, and more than 35 times smaller in terms of free space wavelength area than the previously published MEMS reconfigurable hybrid coupler [20]. The directivity measurement results for the prototype of Concept 1 are shown in Fig. 17(a) showing a directivity between 10 and 20 dB and going above 20 dB only in actuation State 1 for the relatively narrow band between 10 and 12.5 GHz. The prototype directional coupler of Concept 2 achieves a directivity well above 20 dB in the entire frequency bandwidth for both actuation States 1 and 2, as shown in Fig. 17(b). For State 2 the measured directivity is above 40 dB throughout the whole frequency band from 10 to 18 GHz, which is unparalleled in literature, and emphasizes the performance potential of the novel tuning Concept 2.

D. MEMS actuator and lifetime characterization

Table I shows the measured and simulated actuation and release voltages of the MEMS actuators. For the prototype devices of Concept 1, State 1 is passive, i.e. actuation voltage is only required to maintain the coupler in State 2. For the prototype devices of Concept 2, both states are active, i.e. either one of the two actuators requires actuation voltage to maintain both State 1 and State 2. Despite utilizing stiff

TABLE I
MEASURED AND SIMULATED ACTUATION AND RELEASE VOLTAGES FOR THE PROTOTYPE DEVICES. CONCEPT 1 UTILIZES ONLY ONE ACTUATOR, WHEREAS CONCEPT 2 REQUIRES TWO ACTUATORS OPERATED ALTERNATIVELY IN THE TWO STATES.

Measurement Data	**Concept 1**	**Concept 2**	
State 1		**Actuator 1**	**Actuator 2**
Actuation Voltage (V)	0	28	0
Release Voltage (V)	0	23	0
State 2		**Actuator 1**	**Actuator 2**
Actuation Voltage (V)	35	0	34
Release Voltage (V)	25	0	25

Simulation Data	**Concept 1**	**Concept 2**	
State 1		**Actuator 1**	**Actuator 2**
Actuation Voltage (V)	0	34	0
State 2		**Actuator 1**	**Actuator 2**
Actuation Voltage (V)	34	0	34
Spring Constant (N/m)	49	37	57

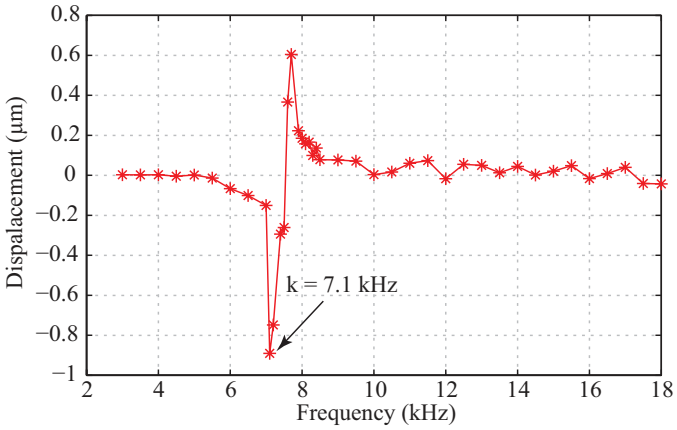

Fig. 18. Measurements of mechanical resonance frequency of the actuator using a white light interferometer.

mechanical spring designs, reasonable actuation voltages with a maximum around 35 V are sufficient to operate the devices. The measured actuation voltages agree very well with the simulation except for the deviation in the actuation voltage of actuator 1 of Concept 2. The actuation voltages are very reproducible with a standard deviation of 0.043 V for 100 subsequent actuation cycles. For the release voltage, the standard deviation of 100 subsequent measurements is 1.305 V. As these devices comprise all-metal designs without dielectric layers, neither stiction nor variations in operation voltage was observed during the tests. Fig. 18 shows the mechanical resonance response with a measured resonance frequency of 7.1 kHz of actuator 1 of Concept 2. The actuation due to external shock has been analyzed for the mass-spring model of the actuators for Concept 1 and Concept 2. Actuation due to external shock would occur at external acceleration of 11×10^3 m/s^2 for actuator of device Concept 1. While for the device Concept 2 actuation due to external shock would occur

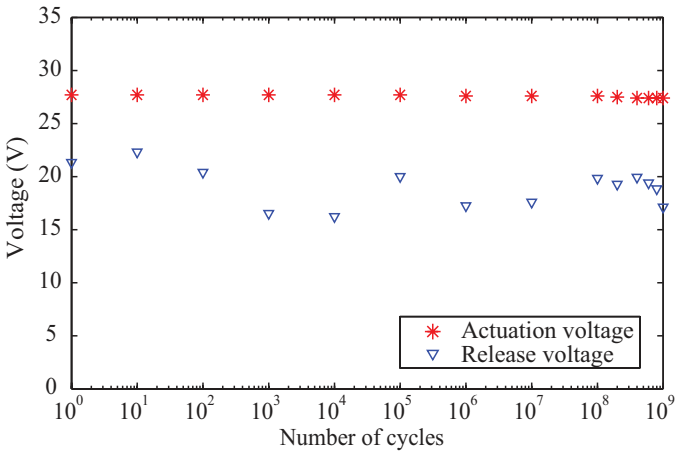

Fig. 19. Life-time characterization: Pull-in and pull-out voltages monitored over 1 billion cycles with 35 V unipolar square waveform with a 50 % duty cycle and a cycle frequency of 1.6 kHz for measuring the pullin/ pull-out actuation hysteresis for each data point.

at external acceleration of 18.1×10^3 m/s^2 for actuator 1, and 11.6×10^3 m/s^2 for actuator 2, respectively.

This type of all-metal, i.e. dielectric-less, RF MEMS device with a monocrystalline-silicon core for all mechanically moving parts is expected to exhibit high reliability similar to other devices of similar mechanical actuator construction developed and evaluated by the authors for their lifetime [22], [23], [31]. Even though the RF signal path is not switched directly, the devices can be classified as contact-mode MEMS devices, since the operation mechanism comprises moving a floating metal block between the signal and the ground line into contact with mechanical stoppers, which potentially bears the risk of contact stiction. Lifetime measurements were performed under "cold" conditions (no RF signal applied) using an unpackaged chip on a probe station in a non-hermetic, uncontrolled atmospheric laboratory environment. The device was actuated using a unipolar 35 V (20% overdrive as compared to measured pull-in voltage of 28 V) square waveform with a 50% duty cycle and a frequency of 1.6 kHz. The pull-in and pull-out hysteresis curves were monitored after each decade of actuation cycles, to derive the pull-in and pull-out voltages over the lifetime. The actuation and release voltage values averaged from three actuation cycles at each measurement point are shown in Fig. 19. The measurements were stopped after 8 days with 87 hours of accumulated pull-in time when one billion cycles were reached without observing any failure or fatigue despite the device being unpackaged. Furthermore, the device did not show any degradation in actuation voltage behavior after one billion cycles. The actuation voltages were very reproducible with a standard deviation of 0.13 V over the one billion actuation cycles calculated using data from Fig. 19. For the releases voltage, the standard deviation over one billion cycles is 1.844 V. Packaging the device would improve the reliability along with the response time.

Finally, Table II summarizes the performance of the designed directional couplers along with the list of various published couplers. These include active MMIC couplers, varactor tuned couplers and MEMS based directional couplers.

TABLE II
PERFORMANCE COMPARISON OF VARIOUS PUBLISHED DIRECTIONAL COUPLERS

Device Technology	Through port (dB)	Coupled port (dB)	Return loss (dB)	Isolation (dB)	Directivity (dB)	Frequency (GHz)	Bandwidth (MHz)	Size[a] (λ)
CMOS MMIC [5]	1.2	3 to -6	>19	>9	>10	6.8	2300	0.03×0.01
GaAs MMIC [14]	-	-60 to -6.6	>9	>9	-	2	500	0.02×0.01
Varactor Diode [10]	-	10 to 6	>15	>15	>10	1.5	1000	0.21×0.12[b]
Varactor Diode [11]	2 to 6	11 to 3	>20	>20	-	2	400	–
Varactor Diode [12]	0.6 to 5	15 to 2	>25	>23	-	2	800	–
MEMS [20]	2 to 25	25 to 2	>16	>17	-	12	400	0.48×0.48
MEMS [21]	-	17 to 10	>10	>13	-	18	4000	0.08×0.07
MEMS (Concept 1)	**4.15 to 5.37**	**8.07 to 6.28**	$\mathbf{>10}$	$\mathbf{>15}$	$\mathbf{>10}$	**14**	**8000**	$\mathbf{0.09 \times 0.06}$
MEMS (Concept 2)	**2.03 to 3.27**	**18.57 to 11.31**	$\mathbf{>15}$	$\mathbf{>40}$	$\mathbf{>22}$	**14**	**8000**	$\mathbf{0.08 \times 0.06}$

[a]Calculated using free space wavelength at the center frequency
[b]Estimated from the figure provided in the paper

VI. CONCLUSION

A novel concept of RF MEMS ultra-wideband 10 to 18 GHz tunable coupled line directional coupler has been presented. Two different tuning concepts involving tuning the distance between the signal lines and the distance of the signal lines to ground were compared. Designs were fabricated and evaluated using the measured RF performance and actuator characterization. The most suitable technology is identified and measurements of the prototypes show excellent tuning results.

ACKNOWLEDGMENT

The authors would like to thank Kjell Noren, KTH, for his help with the critical point dryer utilized in the device fabrication.

REFERENCES

[1] L. K. Yeung and Y. E. Wang, "Mode-based beamforming arrays for miniaturized platforms," *IEEE Trans. Microw. Theory Tech.*, vol. 57, no. 1, pp. 45–52, Jan. 2009.

[2] J. Madic, P. Bretchko, S. Zhang, R. Shumovich, and R. McMorrow, "Accurate power control technique for handset PA modules with integrated directional couplers," in *IEEE MTT-S Int. Microw. Symp. Dig.*, 2003, pp. A201–A204.

[3] L. C. Godara, "Application of antenna arrays to mobile communications, part ii: Beam-forming and direction-of-arrival considerations," *Proceedings of the IEEE*, vol. 85, no. 8, pp. 1195–1245, Aug. 1997.

[4] T. Zelder, E. V. Lluch, B. Geck, I. Rolfes, and H. Eul, "Tunable directional coupler," in *Proc. German Microw. Conf.*, 2008, pp. 1–4.

[5] B. Hur and W. R. Eisenstadt, "Tunable broadband MMIC active directional coupler," *IEEE Trans. Microw. Theory Tech.*, vol. 61, no. 1, pp. 168–176, Jan. 2013.

[6] C.-S. Kim, J.-S. Park, D. Ahn, and J.-B. Lim, "Variable directional coupler with LC resonator," *Electron. Lett.*, vol. 36, no. 18, pp. 1557–1559, Aug. 2000.

[7] G. M. Rebeiz, K. Entesari, I. Reines, S.-J. Park, M. A. El-Tanani, A. Grichener, and A. R. Brown, "Tuning in to RF MEMS," *IEEE Microw. Mag.*, vol. 10, no. 5, pp. 55–72, Oct. 2009.

[8] C.-S. Kim, C.-S.Yoon, J.-S. Park, D. Ahn, J.-B. Lim, and S.-I.Yang, "A design of the novel varactor tuned directional coupler," in *IEEE MTT-S Int. Microw. Symp. Dig.*, 1999, pp. 1725–1728.

[9] S. Toyoda, "Variable coupling directional couplers using varactor diodes," in *IEEE MTT-S Int. Microw. Symp. Dig.*, 1982, pp. 419–421.

[10] S.-M.Wang, C.-Y. Chang, and J. Lin, "A software configurable coupler with programmable coupling coefficient," in *IEEE MTT-S Int. Microw. Symp. Dig.*, 2007, pp. 185–188.

[11] L. K. Yeung, "A compact directional coupler with tunable coupling ratio using coupled-line sections," in *Proc. Asia Pacific Microw. Conf.*, 2011, pp. 1730–1733.

[12] T. Lehmann, H. Mextorf, and R. Knoechel, "Design of quadrature directional couplers with continuously variable coupling ratios," in *Proc. European Microw. Conf.*, 2008, pp. 199–202.

[13] M. A. Y. Abdalla, K. Phang, and G. V. Eleftheriades, "A compact highly reconfigurable CMOS MMIC directional coupler," *IEEE Trans. Microw. Theory Tech.*, vol. 56, no. 2, pp. 305–319, Feb. 2008.

[14] R. Scheeler and Z. Popovic, "GaAs MMIC tunable directional coupler," in *IEEE MTT-S Int. Microw. Symp. Dig.*, 2012, pp. 1–3.

[15] R. V. Gatti, A. Ocera, S. Bastioli, L. Marcaccioli, and R. Sorrentino, "A novel compact dual band reconfigurable power divider for smart antenna systems," in *IEEE MTT-S Int. Microw. Symp. Dig.*, 2007, pp. 423–426.

[16] K. M. Cheng and S. Yeung, "A novel rat-race coupler with tunable power dividing ratio, ideal port isolation, and return loss performance," *IEEE Trans. Microw. Theory Tech.*, vol. 61, no. 1, pp. 55–60, Jan. 2013.

[17] G. M. Rebeiz, *RF MEMS Theory, Design, and Technology*. NewYork: Wiley, 2003.

[18] V. T. Vo, L. Krishnamurthy, Q. Sun, and A. A. Rezazadeh, "3-D low-loss coplanar waveguide transmission lines in multilayer MMICs," *IEEE Trans. Microw. Theory Tech.*, vol. 54, no. 6, pp. 2864–2871, Jun. 2006.

[19] N. J. Farcich and P. Asbeck, "A three-dimensional transmission line with coplanar waveguide features," *Microw. and Optical Technol. Lett.*, vol. 48, no. 11, pp. 2189–2192, Nov. 2006.

[20] A. Ocera, P. Farinelli, F. Cherubinil, P. Mezzanottel, R. Sorrentino, B. Margesin, and F. Giacomozzi, "A MEMS-reconfigurable power divider on high resistivity silicon substrate," in *IEEE MTT-S Int. Microw. Symp. Dig.*, 2007, pp. 501–504.

[21] L. Marcaccioli, P. Farinelli, M. M. Tentzeris, J. Papapolymerou, and R. Sorrentino, "Design of a broadband MEMS-based reconfigurable coupler in ku-band," in *Proc. European Microw. Conf.*, 2008, pp. 595–598.

[22] U. Shah, M. Sterner, and J. Oberhammer, "Multi-position RF MEMS tunable capacitors using laterally moving sidewalls of 3-D micromachined transmission lines," *IEEE Trans. Microw. Theory Tech.*, vol. 61, no. 6, pp. 2340–2352, Jun. 2013.

[23] M. Sterner, N. Roxhed, G. Stemme, and J. Oberhammer, "Static zero-power-consumption coplanar waveguide embedded DC-to-RF metal-contact MEMS switches in two-port and three-port configuration," *IEEE Trans. Electron Devices*, vol. 57, no. 7, pp. 1659–1669, Jul. 2010.

[24] U. Shah, M. Sterner, and J. Oberhammer, "Compact MEMS reconfigurable ultra-wideband 1018 Ghz directional couplers," in *IEEE Int. Conf. Micro Electro Mechanical Systems*, Jan. 2012, pp. 684–687.

[25] D. M. Pozar, *Microwave Engineering*. NewYork: Wiley, 2005.

[26] T. Makita, I. Tamai, and S. Seki, "Coplanar waveguides on high–resistivity silicon substrates with attenuation constant lower than 1 dB/mm for microwave and millimeter–wave bands," *IEEE Trans. Electron Devices*, vol. 58, no. 3, pp. 709–715, Mar. 2011.

[27] M. Sterner, N. Roxhed, G. Stemme, and J. Oberhammer, "Electrochemically assisted maskless selective removal of metal layers for three-dimensional micromachined SOI RF MEMS transmission lines and

devices," *J. Microelectromech. Syst.*, vol. 20, no. 4, pp. 899–908, Aug. 2011.
[28] "CH02016 High frequency 50 Ghz thin film chip resistor," Vishay Sfernice, 63 Lancaster Avenue Malvern, PA 19355-2143, USA.
[29] J. M. Oliver, H. Kazemi, J. Rollin, D. Sherrer, S. Huettner, and S. Raman, "Compact, low–loss, micromachined rectangular coaxial millimeterwave power combining networks," in *IEEE MTT-S Int. Microw. Symp. Dig.*, 2013, pp. 1–4.
[30] R. N. Simons, *Coplanar Waveguide Circuits, Components, and Systems*. NewYork: Wiley, 2001.
[31] N. Somjit, G. Stemme, and J. Oberhammer, "Power handling analysis of high-power W-band all-silicon MEMS phase shifters," *IEEE Trans. Electron Devices*, vol. 58, no. 5, pp. 1548–1555, May 2011.

Umer Shah (S'09) was born in Bannu, Pakistan, in 1981. He received the B.S. degree in engineering from the GIK Institute, Topi, Pakistan, in 2003, and the Masters of Science degree in wireless engineering (with an emphasis on RF integrated circuits (RFICs), monolithic microwave integrated circuits (MMICs), and antenna design) from the Technical University of Denmark (DTU), Copenhagen, Denmark, in 2007.

He spent one year as a Researcher with the GIK Institute prior to earning theMasters in Science degree. His Masters thesis research was with Interactive Sports Games (ISG) A/S. Following theMasters of Science degree, he was involved with the development of satellite front ends with a research organization. Since December 2008, he has been a Ph.D. student with the MST Group, KTH Royal Institute of Technology, Stockholm, Sweden. His research focus includes RF MEMS-based filters, phase shifters, matching circuits, and antennas. His further interests includes MMICs, RFICs, and antenna design.

Mr. Shah was the recipient of the Best Student Paper Award presented at the 2010 AsiaPacific Microwave Conference, Yokohama, Japan.

Mikael Sterner was born in Stockholm, Sweden, in 1981. He received the M.Sc. degree in engineering physics from the KTH Royal Institute of Technology, Stockholm, Sweden, in 2006, and is currently working toward the Ph.D. degree in microsystems technology at the KTH Royal Institute of Technology.

Since 2006, he has been with the Microsystem Technology Laboratory, KTH Royal Institute of Technology. His main research fields are RF MEMS switches and microwave MEMS tunable high-impedance surfaces.

Joachim Oberhammer (M'06-SM'12) was born in Brunico, Italy, in 1976. He received the M.Sc. degree in electrical engineering from the Graz University of Technology, Graz, Austria, in 2000, and the Ph.D. degree from the KTH Royal Institute of Technology, Stockholm, Sweden, in 2004. His doctoral research concerned RF MEMS switches and microsystem packaging.

He was involved with automotive sensor electronics and RF identification (RFID) systems with the Graz University of Technology, and the Vienna University of Technology, Vienna, Austria, prior to joining the Microsystem Technology Laboratory, KTH Royal Institute of Technology, Stockholm, Sweden. After having been a Post-Doctoral Research Fellow with the Nanyang Technological University, Singapore, he returned to the KTH Royal Institute of Technology in 2005, as an Assistant Professor. In 2007, he became an Associate Professor with the KTH Royal Institute of Technology, where he heads a research team with activities in RF and microwave MEMS. In 2007, he was a Research Consultant with the Nanyang Technological University. In 2008, he spent seven months as a Guest Researcher with Kyoto University, Kyoto, Japan. He has authored or coauthored over 80 reviewed research papers.He holds four patents.

Dr. Oberhammer was a TPRC member of IEEE Transducers (2009), the IEEE Microwave Theory and Techniques Society (IEEE MTT-S) International Microwave Symposium (IMS) (20102012), and the IEEE Microelectromechanical Systems (2011 and 2012). Since 2009, he has been a Steering Group member of the IEEE MTT-S and Antennas and Propagation (AP-S) Chapters Sweden. He was the recipient of the 2004 and 2007 Ericsson Research Foundation Award and a Swedish Innovation Bridge grant, respectively. He was the recipient of the 2008 Visiting Researcher Scholarship of the Japanese Society for the Promotion of Science. The research he heads was bestowed the Best Paper Award of the IEEE European Microwave Integrated Circuit Conference (2009), a Best Student Paper Award of the IEEE AsiaPacific Microwave Conference (2010), and a Graduate Fellowship Award of the IEEE MTT-S (2010 and 2011).